

Design and Characterization of a Novel High-Compliance Spring for Robots with Soft Joints

F.Negrello¹, M.G.Catalano¹, M.Garabini², M.Poggiani², D.G.Caldwell¹, N.G.Tsagarakis¹ and A.Bicchi^{1,2}

Abstract—Low stiffness elements have a number of applications in Soft Robotics, from Series Elastic Actuators (SEA) to torque sensors for compliant systems.

In its general formulation, the design problem of elastic components is complex and depends on several variables: material properties, load range, shape factor and size constraints.

Consequently, most of the spring designs presented in literature are based on heuristics or are optimized for specific working conditions.

This work presents the design study and characterization of a scalable spoked elastic element with hinge tip constraints.

We compared the proposed design with three existing spring principles, showing that the spoked solution is the convenient option for low-stiffness and low shape factor elastic elements.

Therefore, a design analysis on the main scaling parameters of the spoked spring, namely number of spokes and type of constraints, is presented. Finally, an experimental characterization has been conducted on physical prototypes. The agreement among simulations and experimental results demonstrates the effectiveness of the proposed concept.

I. INTRODUCTION

The introduction of compliance in the joints transmission allows to decouple the inertia of the drive from the inertia of the link, effectively reducing the peak force transmissibility [1][2][3]. At the same time, maximizing the elastic deflection improves the maximum storable energy in the mechanism. Based on this idea many different series elastic (SEA) and variable stiffness actuators (VSA) have been developed [4][5][6]. Generally, these actuators find their applications in legged robots [7][8][9], manipulators [10] and exoskeletons [11], effectively demonstrating robustness in tasks involving cyclic impacts (e.g.hammering) [12][13].

The new generation of robots is required to be equipped with a rich proprioceptive sensory system that provides them with the ability to sense and control their physical interaction with the environment or people. As pointed out in [14], robots safety and dependability should be ensured during physical interactions. This implies a knowledge of the forces exchanged between the robot and the environment to enable suitable controllers to handle safely the contact forces.

The simplest way to measure contact forces occurring in any part of a serial robot manipulator is to provide the robot with joint torque sensors [15]. As [16] suggests, it is

This work is supported by the WALK-MAN FP7-ICT-2013-10 European Commission project.

¹Department of Advanced Robotics, Istituto Italiano di Tecnologia, Via Morego 30, 16163, Italy, {francesca.negrello, manuel.catalano,nikos.tsagarakis, antonio.bicchi, darwin.caldwell}@iit.it

²Research Center “Enrico Piaggio”, University of Pisa, Largo Lucio Lazzarino 1, 56126 Pisa, Italy, {manolo.garabini,mattia.poggiani,bicchi}@centropiaggio.unipi.it

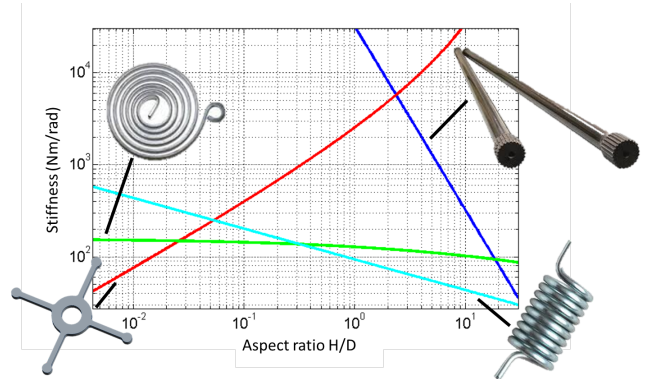


Fig. 1: Analysis of different spring design workspace, for a given set of load and volume constraint.

possible to obtain a torque feedback by directly measuring the deflection of a known stiffness element (spring) using position sensors.

In literature several spring geometries have been presented [17][18]. Commonly, to simplify the problem, a particular geometry is selected and optimized for a specific set of working conditions or to match the stiffness requirements [19]. Still there is not a unified approach for optimal spring shape selection and usually it is based on heuristic criteria.

The general problem of optimizing an elastic element is not easy, the only known quantities in the problem are the applied loads, the admissible support conditions, the volume of the structure and, possibly, some additional design restrictions such as the location and size of prescribed holes or solid areas. Bendsøe et al. [20] discuss how to set-up a general topology optimization. The problem is nonlinear and, in general, nonconvex even in its discretized form. It can be tackled via a careful application of suitable numerical methods. Nevertheless, the solving process is time consuming and not free from possible complications such as: dependency on the mesh-refinement, the checkboard problem, and local minima.

Our goal is to obtain a modular spring geometry for pancake applications that can be easily scaled to match the different requirements of shape factors and load levels. Hence, we prefer to study a geometry that allows an analytical solution within a parametric design.

In Section II we state the problem and we investigate the solution workspace of four analytical cases (namely, torsion bar, helical spring, spiral spring, and spoked spring) found

in literature, as function of the load, volume (parametrized as a cylinder) and shape factor, in order to bound the general problem (Fig. 1).

Simulations demonstrate that for pancake motors applications (shape factor $10^{-3} - 10^{-2}$, loads $10^1 - 10^2$ Nm) the lowest stiffness is provided by the spoked spring. Therefore, this geometry is deeply analyzed in the following sections. The effects of the end constraints on the selected geometry are discussed in Section III, through analytical models. Traditional spoked springs can be modeled as a beam with one end fixed and the second one guided (rotation and radial contraction constrained) which is a two times hyperstatic system (overconstrained). In order to approximate the behavior of a cantilever beam (ideal isostatic system) we propose a hinged tip constraint, aiming to reduce the constraints at the beam end and thus maximize the achievable deflection. This turns into a better utilization of the spring material resulting in a compact, lightweight and modular implementation. This concept at the best of authors' knowledge is new for robotic applications, both for compliant torque sensor, and elastic actuator designs.

Based on these considerations, in Section IV we propose a novel spring with a parametric shape (increasing the length of the spoke) and hinged spoke ends. Tests on physical prototypes (Section V) show that the proposed spring design has a very linear behavior and the hinged end constraint contributes to increase the compliance of about 75% with respect to fixed end constraint for simple spoke geometry. More complex spoke geometries maximize the beam length, therefore the contribution given by the hinged end over the global compliance is reduced, in this case compliance is increased of about 11% with respect to fixed end constraint. Finally, two possible applications of the results presented here, namely a compliant torque sensor and a SEA are reported.

II. PROBLEM DEFINITION

The objective of this work is to identify a geometry suitable for a modular spring implementation, that provides large deflections and that can be easily scaled. Design constraints are, among the others, volume, shape factors, e.g. length-to-width ratio, and load levels.

Aiming to obtain a parametric solution, a size optimization with the following features was considered:

- **Performance Index:** the compliance maximization problem can be stated as a constrained external work maximization problem.
- **Optimization Variables:** spring geometrical parameters.
- **Static Equilibrium Constraint:** an equality constraint in which the external work is equated to the internal elastic energy.
- **Limited Resource Constraints:** i) the available amount of material is constrained assuming that the elastic element is included in a given cylinder of diameter D and height H , ii) the maximum equivalent

stress of the component, $\sigma_{eq}(x)$, which is bounded by the yield stress σ_y .

Note that the values of spring geometrical parameters that solve the size optimization problem are not independent from the material selection. In [21] indices can be found to estimate the upper boundaries imposed on shape efficiency by the material properties (yield stress and elastic modulus).

Four different spring designs were compared: the torsion bar, the spiral spring, the helical spring, and the spoked spring. These have been chosen since they are the principal designs present in the literature.

In the first three cases (namely, torsion bar, spiral spring, helical spring) the solution of the size optimization problem is straightforward (see e.g. [22]).

In the following, the size optimization problem is briefly stated for a spring design with equal spokes of rectangular cross-section; under the assumptions that the total torsion load τ is equally distributed along the spokes and that each spoke behaves like a cantilever beam. The size of the spring is parametrized by the number of spokes N_s . Thus, the size optimization problem becomes:

$$\begin{aligned} & \min_{\theta, b, h, L} \quad -\tau \theta \\ \text{s.t.} \quad & \int_0^L \frac{6M(l)^2}{Ebh^3} dl = \frac{\tau \theta}{N_s} \\ & V = \frac{\pi D^2 H}{4} = \text{const} \quad , \\ & 0 \leq L \leq \frac{D-d}{2} \\ & b \leq H \\ & \frac{12L\tau}{N_s(D-d)bh^2} \leq \sigma_y \\ & \theta \geq 0 \end{aligned} \quad (1)$$

where the angular displacement θ , the length of the spokes L , the width b , and the height h of the spokes represent the optimization variables (Fig. 2). The base diameter of the spokes, d , is fixed. In the static equilibrium constraint the elastic energy of the cantilever beam assumes a simple form where $M(l) = \tau/(N_s L)(L-l)$, and E represents the Young modulus of the material. Last, the inequalities specialize the constraints on volume and stress for the cantilever beam case.

It can be shown that the problem (1) has a unique solution for which the resource constraints are all active, hence $L = (D-d)/2$, $b = H$, $h = \sqrt{12L\tau/(N_s(D-d)H\sigma_y)}$.

The size optimization problem was evaluated for: $V = 10^4 \text{mm}^3$, $10^{-3} \leq H/D \leq 10^2$ and $10^0 \text{Nm} \leq \tau \leq 10^2 \text{Nm}$, the four analyzed cases are represented in Fig.1 and Fig. 3. The results were evaluated for aluminum alloy, analogous considerations can be done for different materials.

Fig. 3 shows the four cases springs stiffnesses as function of different loads and aspect ratio, while Fig. 1 reports a cross section of the 3D plot for a given torque value (30Nm). In general it can be noticed that each design satisfies different

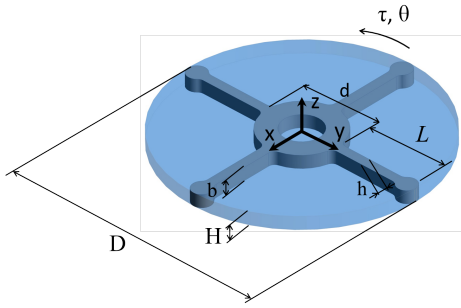


Fig. 2: Spoked spring parametrization.

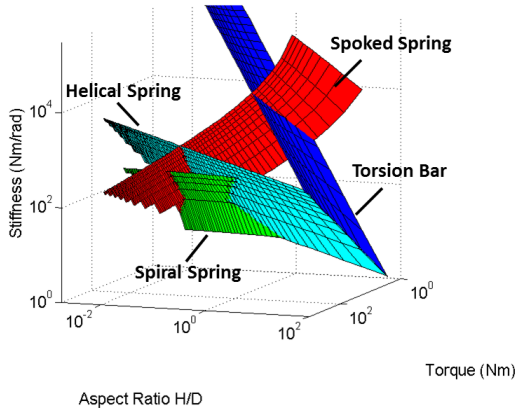


Fig. 3: State of the art springs compared for different load levels and different volume aspect ratio (H/D), the volume is assumed to be cylindrical. The stiffness level of the torsion bar is represented by the blue surface, the cyan is the helical spring, the green the spiral spring, and the red is used for the spoked spring.

application ranges. More in detail, at low shape factor and low loads the spiral spring provides lower stiffness, but it is not a feasible design for high loads ($\tau \leq 10$ Nm). The torsion bar is a good option for high shape factor ($H/D \geq 10^1$) but the helical spring is preferable as soon as the shape factor decreases. The spoked spring is the best choice for low to medium shape factors, and medium to high loads (shape factor $10^{-3} - 10^{-2}$, loads $10^1 - 10^2$ Nm). For example, within the given constraints, for $H/D = 10^{-2}$ a spiral spring provides a stiffness which is twice the spoked spring ones, while the helical spring is 5.7 times higher.

Since the above discussed load ranges and shape factors are useful in many robotic applications (e.g. see Figs. 15-16), in the following parts of the paper the design problem of spoked springs will be extensively studied. In particular the effects of three parameters will be analyzed: i) the constraints on the ends of the spokes, ii) the number of the spokes, and iii) the number of radial segments for each spoke.

III. ANALYTICAL BEAM TIP CONSTRAINT MODEL

In this section we recall shortly the mathematical models, based on the beam theory, to study the effects of the different tip constraint, which are special cases of the general theory. The first model, the cantilever beam (Fig. 4 a), b)), is the isotatic case and represents the maximum deflection for a given load and a given set of parameters (geometrical and material

properties). The beam with one end fixed and the second end guided c), d) (rotation and radial displacement constrained) is the representative scheme of conventional springs for torque sensors [23][24][25]. While the third model (Fig. 4 e), f)), the cantilever with constrained contraction along x axis (hinged end), represents the proposed spring. For second and third case it is worth considering also the axial forces generated by the axial constraint on the beam, which are normally neglected.

From beam theory [26], the equation governing the beam's deflection is (2), which is valid under the following conditions: linear elastic deformation, slender beam (its length to height ratio is greater than 10), small deflections (max deflection less than 1/10 the span).

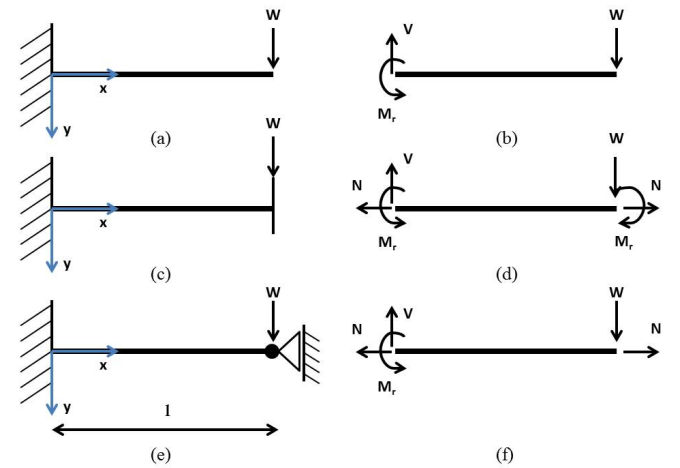


Fig. 4: Beam schemes at different tip constraints and their corresponding load schemes: a) Cantilever beam, c) Cantilever with guided end, e) Cantilever with hinged end.

$$\ddot{y} = \frac{-M}{EJ} \quad (2)$$

where: M is the global bending moment acting on the section (Nmm), E is the Young Modulus of the material (MPa) and J is the area moment of inertia of the cross-section (mm^4).

For the general case of fig. 4, where a load (W) is acting on a cantilever beam with different end constraints, (2) can be written as:

$$\ddot{y} = \frac{M_r - Vx + Ny(x)}{EJ} \quad (3)$$

where: M_r , V and N are the reactive loads, which can be evaluated imposing the equilibrium equations, respectively a moment (Nmm), a vertical force and an axial reactive force in N .

Eq. (4) expresses the boundary conditions of the fixed side of the beam, where rotation and displacement are equal to zero.

$$\dot{y}(0) = y(0) = 0 \quad (4)$$

The guided end introduces two more constraints in the system, both rotation and axial displacement of the beam tip are equal to zero, as expressed by (5). To solve the twice hyperstatic system we refer to the equivalent isostatic system that is obtained by substituting extra constraints with the equivalent reactive loads (Fig.4 d)).

$$\dot{y}(l) = u_x = 0 \quad (5)$$

To evaluate N it is imposed that the displacements along x, due to the deflection, are equal to the elongation produced by N, as expressed by (6), from [27][28]:

$$N = \frac{EA}{l} \int_0^l \dot{y}(x)^2 dx \quad (6)$$

The hinged end, case e) Fig. 4, instead, introduces only the axial displacement constraint as tip condition (7), consequently the system is just one time hyperstatic.

$$u_x = 0. \quad (7)$$

Fig. 5 shows, as an example, the displacements in y direction and the beam tip rotations (\dot{y}) for the three cases studied. In particular for case c) (cantilever with fixed end) the results considering N and neglecting it (analytical solution) are reported. It is possible to evaluate that case e) (Cantilever with pinned end) produces displacement comparable to the cantilever beam and several times larger than case c). As a matter of fact the pin at the end allows to relax the constraints on the beam and provides larger deflections.

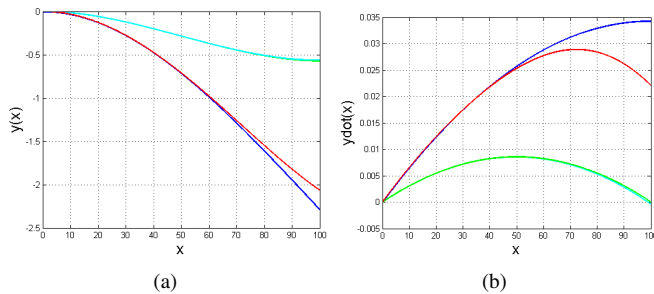


Fig. 5: Comparisons of the models in y (left) and \dot{y} (right), the line colors are as follows: case a)-blue, case c)-green, case c*)-with-N-cyan, case e)-with-N-red

IV. SPRING DESIGN

Based on the above considerations a study on spoked springs with pinned end was developed. Design constraints are represented by inner and outer diameter. It was hypothesized to connect those with N_s spokes, which are designed to maximize the length of the equivalent beam through a series of radial and tangential segments (Fig. 6).

To study the spring geometry, a simplified analytical model, in which the spoke shape has been discretized as a series of beams, has been developed based on the equations presented in the previous section. As first approximation it is assumed that radial parts of the spoke are subjected to

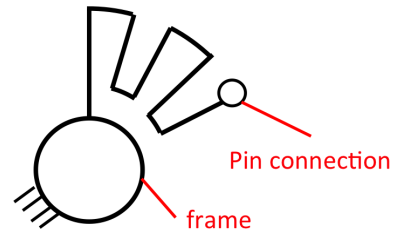


Fig. 6: Proposed spring layout.

bending loads while tangential parts are subjected to normal loads and therefore their contribution is negligible. The aim of this model is to provide a first approximation of the effects of the spokes number (N_s) and of the spoke segments number (N) on the global spring deflection, considering the effects of the constraint on the spoke end.

Note that the geometry of the spoke does not guarantee per se a symmetric behavior with respect to opposite loads (Fig. 7). To ensure symmetry, an even number of spokes with opposite orientation should be employed. In this way half of them is subjected to a load (e.g. clockwise torque) while the other half is subjected to the opposite load.

Another observation is related to the placement of the pin connections. Their location should ensure a balanced transmission of the loads, this implies a bound on the minimum number of spokes $N_s \geq 4$, since $N_s = 2$ would introduce a torque in the plane of the rotation axis. The area that each spoke can occupy is $1/N_s$ of circumference and consequently determines the max spoke segments number (N).

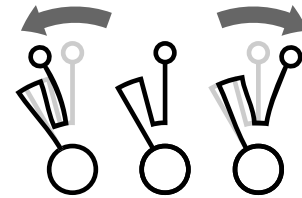


Fig. 7: Sketches of spring deflection when subject to a counter-clockwise torque (CCW), on the left, and to a clockwise torque (CW), on the right.

A constraint on the maximum spoke segments number is given by the deformation of the spring itself under loading conditions, indeed the spokes may get in contact with each other introducing hysteresis as discussed in [23][18].

To study the effects of the different spring parameters a practical case study was considered ($\tau=20\text{Nm}$, $V=10^4\text{mm}^3$, $H/D=5 \cdot 10^{-2}$), which in the next section is validated through experimental tests. In the example the maximum deflection of the segments is evaluated to be about 1.5mm, thus a gap between the spokes of 3mm is considered conservative. These assumptions constrain the maximum number of spoke segments (N) to seven for a four spokes spring (N_s). In Fig. 8(b) and 8(a) the spring deflection of a geometry with $N_s = 4$ spokes is compared to the one with $N_s = 6$

spokes as function of the segments number (N). Albeit the spring with $N_s = 6$ provides larger deflections for $N \leq 4$, the solution with four spokes allows to use more segments, further increasing the spring compliance.

Moreover, geometries with a large number of pin connections may show an asymmetric behavior due to spokes preload caused by mechanical tolerances. This effect can be relevant for high stiffness springs.

Comparing the figures concerning the theoretical deflection of the fixed end (Fig.8(a)) and of the hinged end (Fig.8(b)) it is worth noticing that even for a multi-segment spoked geometry, which offers large deformations, the hinged end solution improves the total spring deflection about the 15%.

Another important aspect is the modularity of the proposed geometry. Since the spring stiffness and stress are directly proportional to the axial length (b), this parameter may be used to scale up a selected design in order to match different loads requirements.

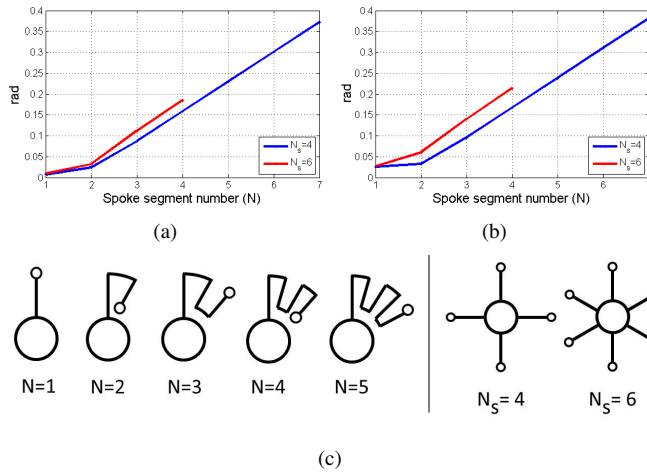


Fig. 8: The graphs report the deflection of the spring as function of the spokes segment number, for both fixed end (left) and hinged end (right). The sequence (c) shows the topology of the spring as function of the number of radial segments (N) and of the number of spokes (N_s).

To evaluate the effectiveness of the proposed solution, a finite element analysis (FEM) was conducted on several geometries to compare the resulting stiffnesses. Fig. 9 shows the different analyzed geometries, a spoked spring with fixed end for $N=1$ (from ref. [29]) and $N=5$ (Fig. 9(a)), the hinged case for $N=1$ and $N=5$ (Figs. 9(b) and 9(d)).

Fig. 9 shows results of the FEM analysis in terms of tangential displacements for the different spring geometries. Comparing the results with the analytical model it is confirmed that the pin constraint increases spring compliance. Note that in the FEM model a triangular spoke geometry was used in order to further optimize the material utilization.

In Tab. I the results of the FEM analysis are reported as: estimated stiffness, max stress and max displacement for the geometries in Fig. 9. FEM has been conducted constraining: external diameter displacements and rotations (Springs Fig.

9(a) and 9(c)), pin holes displacements (Springs Fig. 9(b) 9(d)) and inner diameter radial displacements; torque load has been applied on the inner diameter ($\tau = 10\text{Nm}$).

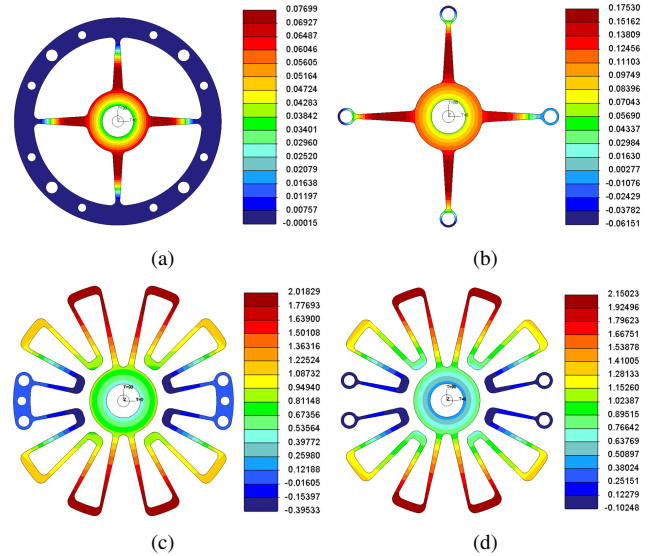


Fig. 9: Tangential displacements for the different spring geometries, in millimeters.

It is interesting to notice that the simpler hinged geometry (Fig. 9(b)) has twice the deflection of the corresponding geometry with fixed ends (Fig. 9(a)).

According to the analytical study, an increment of N (Fig. 9(d)) further improves the spring compliance. In particular through FEM analysis the improvement given by the hinge for the configuration d) ($N=5$, pin constraint) is estimated to be about 10% with respect to the fixed end.

TABLE I: FEM analysis results, for each spring evaluated stiffness, max stress and max displacement are reported. The material used was Aluminum (Al 7075-T6) and external load $\tau = 10\text{Nm}$.

| | A | B | C | D |
|------------------|------|------|------|-------|
| k (Nm/rad) | 2000 | 952 | 140 | 130 |
| max stress (MPa) | 180 | 350 | 340 | 270 |
| max disp. (mrad) | 5.0 | 10.5 | 71.0 | 74.16 |

V. EXPERIMENTAL TESTS

This section describes the set-up conceived to compare spoked springs with different spoke end constraints and different spoke segment number (N). Furthermore, data about their experimental characterization are reported.

A. Set-up

Two set of springs were manufactured by conventional CNC machining, $N = 1$ and $N = 5$, respectively for the fixed and the pinned end (Fig. 11) and with $N_s=4$. The springs used in the test bench have been designed to satisfy the following specifications: $\tau=10\text{Nm}$, $D=85\text{mm}$, the material selected is aluminum (Al 7075-T6) and a safety factor $SF = 2$ has been considered.

In the set-up (Fig. 10) the tested spring is on one side fixed to the frame, while on the other, it is linked to a commercial geared motor (Maxon DCX35). The spring deflection is measured with a 19bit magnetic encoder (Renishaw AKSIM) while a commercial 6 axis F/T sensor (ATI MINI-58) is connected in series with the spring to provide a torque reference (Fig. 10). Both the position and the F/T sensor are sampled at 500Hz.

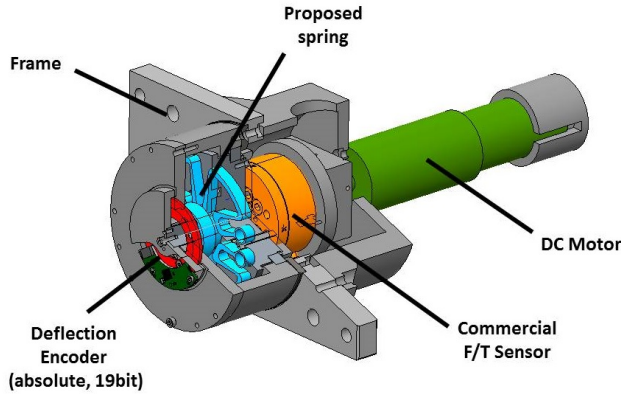


Fig. 10: Cross-section 3D view of the experimental set-up. The figure shows: the motor, the off-the-shelf F/T sensor, the designed spring, and the high resolution position sensors.

B. Results

Tests were carried out on each spring to characterize their stiffness and to investigate their behavior as function of the frequency and of the amplitude of the sinusoidal input provided by the motor.

1) *Calibration*: Fig. 13 shows the deflection of the springs with respect to the applied torque from -10Nm to 10Nm. It is worth noticing the linear behavior of the springs. Spring B shows a slight flattening about zero torque, which is caused by clearance in the pin connections.

Data has been acquired applying a sinusoidal torque profile at low frequency (0.1Hz for A-B and 0.001Hz for C-D) with a sampling time of 2ms. Each curve has been evaluated on 2 load cycles. The evaluated stiffness and other statistical indexes are reported for each spring in Tab. II.

Experimental results confirm the benefits of the pin constraint discussed in Sec. III. The analytical model (Fig. 5(a)) estimates for $N=1$ K_B is $1/4K_A$, while experimentally K_A is $3.66K_B$. Increasing the spoke segment number ($N=5$), and thus the length of the beam, the effect of the hinge constraint is naturally less relevant with respect to the total deflection, still it provides 11% of stiffness reduction, in agreement with FEM.

2) *Hysteresis*: it has been investigated both as function of the load frequency and of the load level. Fig. 12 shows the hysteresis for a sinusoidal load applied with different frequencies, 0.1-1-2Hz for springs A-B (Fig. 12(a) 12(b)) and 0.001-0.02-0.05Hz for springs C-D (Fig. 12(c) 12(d)). The selection of different frequencies has been done to avoid resonance phenomena due to the different springs stiffnesses.

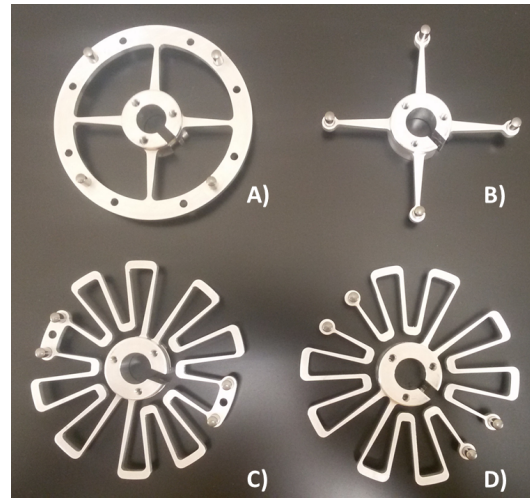


Fig. 11: Tested springs: A) $N=1$ fixed end, B) $N=1$ hinged end, C) $N=5$ fixed end, D) $N=5$ hinged end.

TABLE II: Calibration data, for each spring the experimentally measured stiffness is reported with other statistical coefficient, to evaluate the correctness of the stiffness linearization.

| | A | B | C | D |
|--------------------|---------|--------|--------|---------|
| Stiffness (Nm/rad) | 3856 | 1054 | 101.5 | 89.52 |
| SSE | 54.99 | 1246 | 15820 | 3361 |
| R-Square | 0.999 | 0.997 | 0.999 | 0.999 |
| RMSE | 0.07417 | 0.3531 | 0.1258 | 0.05798 |

Fig. 14 shows the hysteresis for sinusoidal with different amplitude (freq. 0.05Hz), 0.017-0.035-0.07rad for springs C-D (Fig. 14(a)-14(b)).

For each case the load cycle has been repeated 4 times, the max amplitude between loading and unloading phase of the hysteresis loops for the four spring tested is reported in Tab. III.

TABLE III: Hysteresis loop amplitude in radians for the reported frequencies and amplitudes.

| | A | B | C | D |
|--------|--------------------------|---------------------------|--------------------------|--------------------------|
| Freq.1 | $\pm 7.0 \times 10^{-6}$ | $\pm 9.5 \times 10^{-5}$ | $\pm 1.6 \times 10^{-3}$ | $\pm 6.5 \times 10^{-4}$ |
| Freq.2 | $\pm 1.2 \times 10^{-4}$ | $\pm 2.3 \times 10^{-4}$ | $\pm 2.0 \times 10^{-3}$ | $\pm 6.0 \times 10^{-4}$ |
| Freq.3 | $\pm 2.0 \times 10^{-4}$ | $\pm 5.0 \times 10^{-4}$ | $\pm 2.0 \times 10^{-3}$ | $\pm 8.2 \times 10^{-4}$ |
| Ampl.1 | $\pm 1.5 \times 10^{-4}$ | $\pm 5.19 \times 10^{-4}$ | $\pm 2.0 \times 10^{-3}$ | $\pm 2.3 \times 10^{-2}$ |
| Ampl.2 | $\pm 1.0 \times 10^{-4}$ | $\pm 4.2 \times 10^{-3}$ | $\pm 1.3 \times 10^{-3}$ | $\pm 2.8 \times 10^{-4}$ |
| Ampl.3 | $\pm 3.8 \times 10^{-5}$ | $\pm 3.2 \times 10^{-4}$ | $\pm 1.2 \times 10^{-3}$ | $\pm 3.4 \times 10^{-4}$ |

VI. CONCLUSIONS

We presented a novel modular spring design for pancake applications that provides minimum stiffness within a set of design constraints, such as, load level, volume and aspect ratio. In the paper, the selection of the geometry is discussed with respect to other springs presented in literature. Therefore, a detailed study of the effects of the different design parameters is reported (spoke end constraint, number of spokes and number of radial segments composing each spoke).

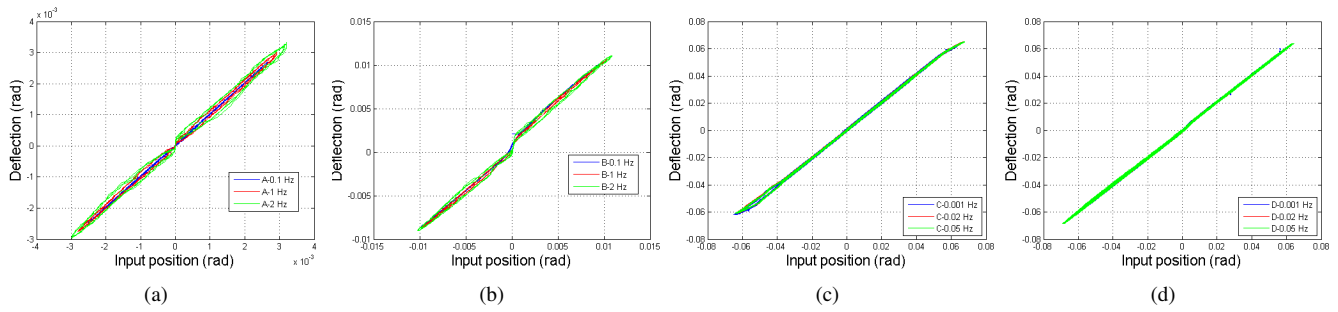
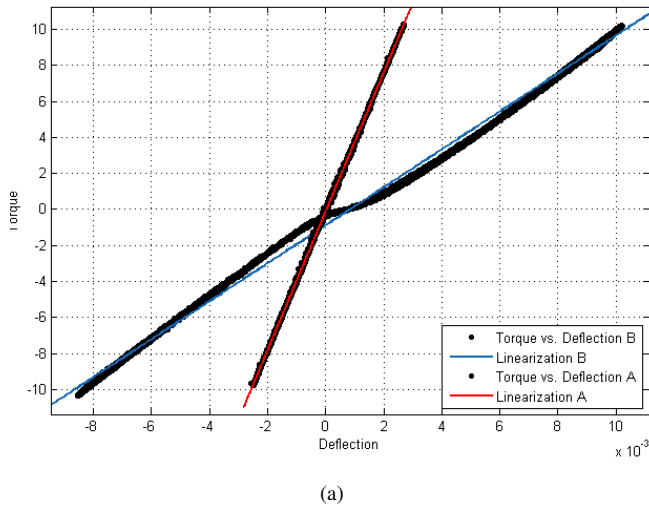
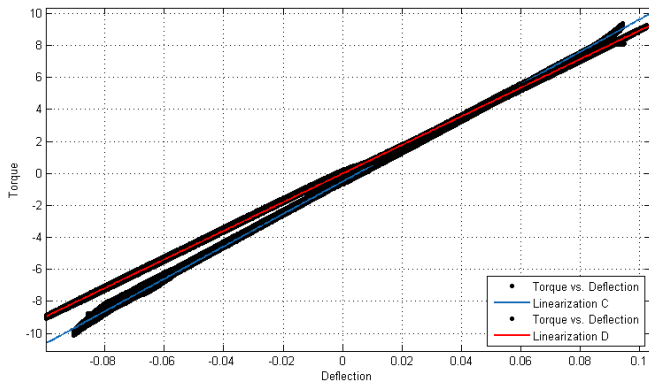


Fig. 12: Hysteresis loop at different frequencies for the tested springs.



(a)



(b)

Fig. 13: Torque (Nm) vs. Deflection (rad). Calibration curves for springs A-B-C-D (as indicated in Fig. 11).

The proposed spring design is based on the hinged end constraint that allows the spoke to approximate the behavior of a cantilever beam (ideal isostatic system) maximizing thus the achievable deflection.

The effectiveness of the proposed spring layout and constraint type was validated experimentally, comparing prototypes of the hinged end spring for $N=1$ and $N=5$, with the equivalent cases with fixed spoke end. Tests on physical

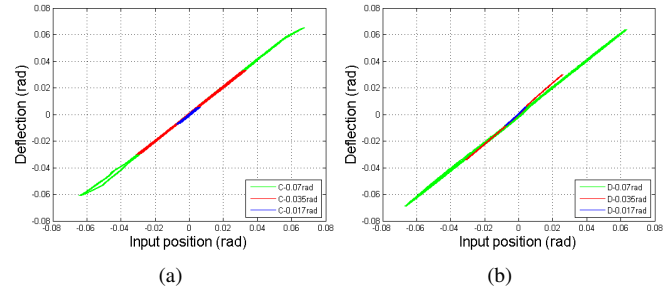


Fig. 14: hysteresis for the four proposed spring geometries as function of the input sine amplitude. Tested amplitude are reported in the legend for each geometry.

prototypes show that the proposed spring design has a very linear behavior and the hinged end constraint contributes to improve the compliance of about 75% with respect to fixed end constraint for the simpler spoke geometry ($N=1$), while it reduces the stiffness of about 11% for more complex spoke geometry ($N=5$). It turns out that the parametrization of the proposed spring makes this geometry easy to be scaled in order to match requirements for different applications. Fig. 15 and 16 show possible implementations for the proposed spring, such as compliant module for series elastic actuator or compliant torque sensor module. For these applications a spring with minimum stiffness on one side offers improved torque resolution while on the other side gives a better utilization of the spring material resulting in a compact, lightweight and modular implementation.

ACKNOWLEDGMENT

The authors want to thank Andrea di Basco for his valuable support in the development of the hardware prototype.

REFERENCES

- [1] Gill A. Pratt, Matthew M. Williamson, P. Dillworth, J. Pratt, and A. Wright. Stiffness isn't everything. In *International Symposium on Experimental Robotics (ISER 1995)*, pages 253–262, Stanford, California, USA, 1995.
- [2] G.A. Pratt and M.M. Williamson. Series elastic actuators. In *IEEE/RSJ International Conference on Intelligent Robots and Systems—Workshop on 'Human Robot Interaction and Cooperative Robots'*, volume 1, pages 399–406, Pittsburg, USA, 1995.
- [3] A. Bicchi and G. Tonietti. Fast and "soft-arm" tactics [robot arm design]. *Robotics Automation Magazine, IEEE*, 11(2):22–33, June 2004.

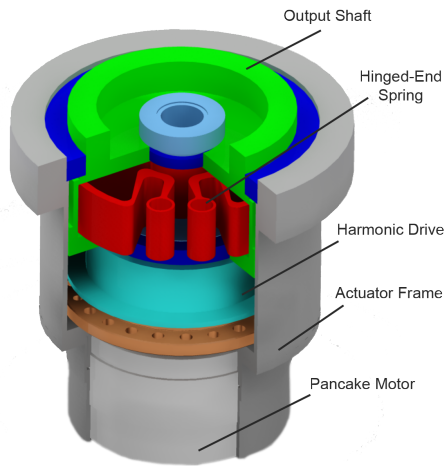


Fig. 15: Example of application of the novel spring in a Series Elastic Actuator (SEA). The spring design has been scaled up in order to transmit torque about 200Nm. In this case the elastic element serves different purposes: embedding compliance and implementing a torque sensor through the measurement of the elastic element deflection under loading.

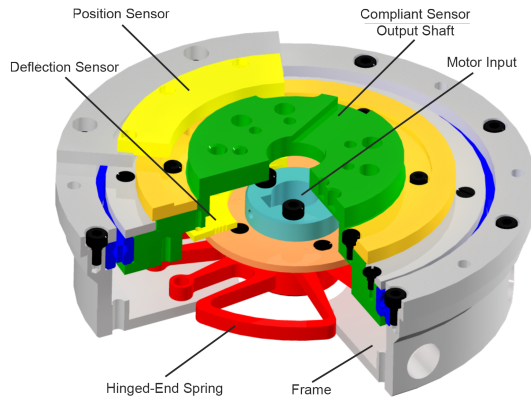


Fig. 16: Example of application of the novel spring in a modular torque sensor (max. torque 10Nm).

[4] R. Van Ham, B. Vanderborght, M. Van Damme, B. Verrelst, and D. Lefeber. Macepa: the mechanically adjustable compliance and controllable equilibrium position actuator for 'controlled passive walking'. In *Robotics and Automation, 2006. ICRA 2006. Proceedings 2006 IEEE International Conference on*, pages 2195–2200, May 2006.

[5] NG Tsagarakis, M. Laffranchi, B. Vanderborght, and D.G. Caldwell. A compact soft actuator unit for small scale human friendly robots. In *IEEE International Conference on Robotics and Automation*, pages 4356–4362. IEEE, 2009.

[6] C.A. Ihrke, J.S. Mehling, A.H. Parsons, B.K. Griffith, N.A. Radford, F.N. Permenter, D.R. Davis, R.O. Ambrose, and L.Q. Junkin. Rotary series elastic actuator, March 24 2011. US Patent App. 12/564,090.

[7] A. Parmiggiani, G. Metta, and N. Tsagarakis. The mechatronic design of the new legs of the icub robot. In *Humanoid Robots (Humanoids), 2012 12th IEEE-RAS International Conference on*, pages 481–486, Nov 2012.

[8] N.G. Tsagarakis, S. Morfey, G.M. Cerda, Li Zhibin, and D.G. Caldwell. Compliant humanoid coman: Optimal joint stiffness tuning for modal frequency control. In *Robotics and Automation (ICRA), 2013 IEEE International Conference on*, pages 673–678, May 2013.

[9] C. Knabe, J. Seminatore, J. Webb, M. Hopkins, T. Furukawa, A. Leonessa, and B. Lattimer. Design of a series elastic humanoid for the darpa robotics challenge. In *Humanoid Robots (Humanoids), 2015 IEEE-RAS 15th International Conference on*, pages 738–743,

Nov 2015.

[10] A. Edsinger-Gonzales and J. Weber. Domo: a force sensing humanoid robot for manipulation research. In *Humanoid Robots, 2004 4th IEEE/RAS International Conference on*, volume 1, pages 273–291 Vol. 1, Nov 2004.

[11] M. Cestari, D. Sanz-Merodio, J.C. Arevalo, and E. Garcia. An adjustable compliant joint for lower-limb exoskeletons. *Mechatronics, IEEE/ASME Transactions on*, 20(2):889–898, April 2015.

[12] M. Grebenstein, A. Albu-Schaffer, Thomas Bahls, M. Chalon, O. Eiberger, W. Friedl, R. Gruber, S. Haddadin, U. Hagn, R. Haslinger, H. Hoppner, S. Jorg, Mathias Nickl, Alexander Nothhelfer, F. Petit, J. Reill, N. Seitz, T. Wimbock, S. Wolf, T. Wusthoff, and G. Hirzinger. The dlr hand arm system. In *Robotics and Automation (ICRA), 2011 IEEE International Conference on*, pages 3175–3182, May 2011.

[13] Markus Grebenstein, Maxime Chalon, Werner Friedl, Sami Haddadin, Thomas Wimböck, Gerd Hirzinger, and Roland Siegwart. The hand of the dlr hand arm system: Designed for interaction. *The International Journal of Robotics Research*, 31(13):1531–1555, 2012.

[14] Agostino De Santis, Bruno Siciliano, Alessandro De Luca, and Antonio Bicchi. An atlas of physical humanrobot interaction. *Mechanism and Machine Theory*, 43(3):253 – 270, 2008.

[15] E. Magrini, F. Flacco, and A. De Luca. Estimation of contact forces using a virtual force sensor. In *2014 IEEE/RSJ International Conference on Intelligent Robots and Systems*, pages 2126–2133, Sept 2014.

[16] D.W. Robinson, J.E. Pratt, D.J. Paluska, and G.A. Pratt. Series elastic actuator development for a biomimetic walking robot. In *Advanced Intelligent Mechatronics, 1999. Proceedings. 1999 IEEE/ASME International Conference on*, pages 561–568, 1999.

[17] F. Sergi, D. Accoto, G. Carpinio, N.L. Tagliamonte, and E. Guglielmelli. Design and characterization of a compact rotary series elastic actuator for knee assistance during overground walking. In *Biomedical Robotics and Biomechanics (BioRob), 2012 4th IEEE RAS EMBS International Conference on*, pages 1931–1936, June 2012.

[18] C. Lagoda, A.C. Schouten, A.H.A. Stienen, E.E.G. Hekman, and H. van der Kooij. Design of an electric series elastic actuated joint for robotic gait rehabilitation training. In *Biomedical Robotics and Biomechanics (BioRob), 2010 3rd IEEE RAS and EMBS International Conference on*, pages 21–26, Sept 2010.

[19] Y. Kim, J. Lee, and J. Park. Compliant joint actuator with dual spiral springs. *IEEE/ASME Transactions on Mechatronics*, 18(6):1839–1844, Dec 2013.

[20] M.P. Bendsoe and O. Sigmund. *Topology Optimization: Theory, Methods, and Applications*. Engineering online library. Springer Berlin Heidelberg, 2003.

[21] Michael F. Ashby. *Materials Selection in Mechanical Design, Fourth Edition*. Butterworth-Heinemann, 4 edition, 2010.

[22] A.M. Wahl. *Mechanical Springs*. [Machine design series]. Penton Publishing Company, 1944.

[23] A.H.A. Stienen, E.E.G. Hekman, H. ter Braak, A.M.M. Aalsma, F.C.T. van der Helm, and H. van der Kooij. Design of a rotational hydro-elastic actuator for an active upper-extremity rehabilitation exoskeleton. In *Biomedical Robotics and Biomechanics, 2008. BioRob 2008. 2nd IEEE RAS EMBS International Conference on*, pages 881–888, Oct 2008.

[24] A. Albu-Schaffer, O. Eiberger, M. Grebenstein, S. Haddadin, C. Ott, T. Wimbock, S. Wolf, and G. Hirzinger. Soft robotics. *Robotics Automation Magazine, IEEE*, 15(3):20–30, September 2008.

[25] Nicholas Paine, Joshua S. Mehling, James Holley, Nicolaus A. Radford, Gwendolyn Johnson, Chien-Liang Fok, and Luis Sentis. Actuator control for the nasa-jsc valkyrie humanoid robot: A decoupled dynamics approach for torque control of series elastic robots. *Journal of Field Robotics*, 32(3):378–396, 2015.

[26] S. Timoshenko. *Strength of materials*. Number v. 1 in Strength of Materials. Van Nostrand, 1955.

[27] R. Parnes. Bending of an axially constrained beam. *International Journal of Mechanical Sciences*, 13(4):285 – 290, 1971.

[28] DasGupta SS Koeneman JB. The bending problem of axially constrained beams. *ASME. J. Eng. Ind.*, 97(1):33–36, 1975.

[29] D. Vischer and O. Khatib. Design and development of high-performance torque-controlled joints. *IEEE Transactions on Robotics and Automation*, 11(4):537–544, Aug 1995.